DOI 10.1007/s10812-023-01486-x
Journal of Applied Spectroscopy, Vol. 89, No. 6, January, 2023 (Russian Original Vol. 89, No. 6, November–December, 2022)

MULTI-ELEMENT DETERMINATION OF FERROCHROMIUM BY ENERGY-DISPERSIVE X-RAY FLUORESCENCE SPECTROMETRY BASED ON DESIGN OF EXPERIMENTS

X. Q. Li,[a,b,c] B. Li,[a,b] Y. P. Dong,[a,b] D. D. Gao,[a,b] W. Li,[a] and H. T. Feng[a,b,*]

UDC 543.42.062

An innovative method for the simultaneous determination of Cr, Fe, Si, Mn, V, Ti, P, and S in ferrochromium was developed based on the powder compression method coupled with energy dispersive X-ray fluorescence spectrometry. The measurement conditions, current, voltage, analytical line, filter, and detector mode were optimized. The optimal sample quality, binder dosage, and tablet pressure were predicted by MINITAB software using a design of experiments that simultaneously investigated the combined effect of the different factors. The matrix and overlapping effects of the element spectrum were corrected using Epslion3 software. The results indicated that the element working curves had a good linear relationship for the selected concentration range, and the correlation coefficient of the eight elements was between 0.9912 and 0.9997. The accuracy of the proposed method was confirmed by analyzing a ferrochromium-certified reference material that had not been used in the linear regression, which ranged from 0.08 to 5.29%. The proposed technique was able to determine the Cr, Fe, Si, Mn, V, Ti, P, and S content of ferrochromium with excellent accuracy and precision, and it was superior to reported methods.

Keywords: *energy dispersive X-ray fluorescence spectrometry, ferrochromium, element analysis, design of experiments.*

Introduction. Ferrochromium, mostly used as an alloy of chromium and iron, is used to produce stainless steel, refractory materials, and chromate compounds [1–3]. In the metallurgical industry, the addition of ferrochromium can effectively enhance strength and hardness while reducing costs. It is a promising additive for the production of low-cost alloys with high mechanical properties [4]. However, the chemical composition of ferrochromium and its trace element content, directly and indirectly, influence the properties and performance of stainless steel and chromium products [5, 6]. Therefore, rapid and robust analytical methods that enable the determination of elements in ferrochromium are crucial for the prompt quality monitoring of alloys and chromium products during the production process. Currently, several analytical techniques are used to assay these products, and the ferrochromium can be evaluated using chemical and spectroscopic methods [7, 8]. However, established methods for the element analysis of the major and trace elements in solid samples, such as chemical titration and inductively coupled optical plasma–atomic emission spectrometry (ICP–AES), have several drawbacks [9]. They require the heating of samples to high temperatures and their dissolution, which makes these methods time consuming and tedious [10, 11]. Moreover, melting the sample dilutes the target elements below the detection limits of the instruments.

X-ray fluorescence (XRF) is an analytical method used to determine the concentration of major and microelements in different matrixes by identifying their composition and content through the energies and intensities of their characteristic X-rays [12, 13]. Compared with ICP–AES, energy dispersive X-ray fluorescence (EDXRF) spectrometry has become popular for the analysis of solid and powder samples [14]. In recent years, it has been demonstrated to be a powerful analytical method for identifying the composition and content of different matrixes owing to its rapid and simultaneous determination of elements [15, 16]. Coedo et al. [17] prepared bulk samples by re-melting ferroalloy diluted with iron in an

*To whom correspondence should be addressed.

[a]Key Laboratory of Comprehensive and Highly Efficient Utilization of Salt Lake Resources, Qinghai Institute of Salt Lakes, Chinese Academy of Sciences, Xining, China; email: 03fht@163.com; [b]Qinghai Engineering and Technology Research Center of Salt Lake Resources Development, Xining, China; [c]University of Chinese Academy of Sciences, Beijing, China. Abstract of article is published in Zhurnal Prikladnoi Spektroskopii, Vol. 89, No. 6, p. 902, November–December, 2022.

induction furnace, and then determined the Cr content of the ferrochromium by XRF and ICP–AES. Wavelength dispersive XRF spectrometry was used by Wang et al. [18] to analyze the chemical compositions and approximate the content of ferrochromium raw materials. Büyükyıldız et al. [19] proposed an approach to the quantitative analysis of Fe–Cr binary ferroalloys using EDXRF, and the characteristic K_α XRF spectra of Fe in a fixed experimental condition. Ferrochromium analytical techniques, however, remain limited to identifying major elements, and few studies have focused on the rapid and accurate multi-element quantification of ferrochromium.

Accordingly, the current study was aimed at developing and validating an EDXRF analytical methodology for the qualitative and quantitative determination of ferrochromium. The counting rate of elements can be affected by the sample particle size, sample quality, binder dosage, and tablet pressure. Although EDXRF sample determination conditions are optimized using univariate optimization or orthogonal experiments, these optimization designs suffer from the impossibility of evaluating the interaction between the studied variables [20]. Therefore, an in-depth study to establish the optimal EDXRF sample preparation conditions for the eight elements analyzed here was crucial to obtaining reliable results with high levels of sensitivity, precision, and accuracy, as well as the lowest limit of detection. Design of experiments (DOE) provides many advantages when determining test conditions under the influence of multiple factors [21, 22]. It can identify the significant factors in a process, the correlation of each factor, and determine the optimal process parameters to achieve the targeted response [23]. However, studies that use DOE to investigate the optimization of EDXRF operational conditions are lacking. Therefore, DOE was used to handle the significant influencing factors while optimizing the operational conditions to improve the measurement precision. The proposed EDXRF method was validated according to related requirements and compared with reported ICP–AES methods.

Experimental. The following analytical grade reagents and chemicals were used: absolute ethanol (Kelong Chemical Co. Ltd., Chengdu, China); high carbon ferrochrome (Wanxiang Metal Alloy Material Co., Ltd., Guizhou, China); microcrystalline cellulose as the selected binder (Macklin Shanghai); and 16 ferrochromium-certified reference materials for the establishment of calibration curves GBW(E)010255–GBW(E)010257, GBW(E)010367–GBW(E)010369, YSBC28621-2010–YSBC28623-2010, YSBC28653-2018–YSBC28657-2018, ZGJT-2013-4, and BH0310-3.

The following instruments were used in the study: a small desktop EDXRF spectrometer (PANalytical B.V. Epsilon 3X), a laser particle size analyzer (BT-9300Z), a vertical planetary ball mill (Changsha Tianchuang QM-0.4A), a desktop electric tablet press (Tianjin Chuang lean), and an inductively coupled optical plasma emission spectrometer (Thermo Fisher Scientific, USA).

A ferrochromium specimen was prepared via a facile pre-processing method, conducted according to the pressed-powder pellet sample method with microcrystalline cellulose [24, 25]. The powder samples were mixed in a ratio of 10:1 in a ball mill with the binder for 10 min, and when the powder sample and microcrystalline cellulose were mixed uniformly, they were pressed into schistose using a pressing machine. After a drift correction was performed with an FLX-C3 glass frit, the pressed samples were analyzed by EDXRF spectrometer. Standard samples were prepared for fluorescence measurements in the same manner as described here for the ordinary samples.

Portions of 0.1000 g ferrochromium were accurately weighed in a 30-mL nickel crucible, and a mixture of 4.0 g potassium hydroxide and 0.4 g potassium nitrate was added to the same container, followed by heating to 700^{o} and melting for 20 min. After the complete decomposition of the sample, it was placed in hot water to soak the frit. Then, 10 mL of ultrapure water and hydrochloric acid were added to the sample solution, which was diluted to the desired volume with ultra-pure water. ICP–AES was used to detect Cr, Fe, Si, V, Ti, and Mn.

Results and Discussion. *Optimization of instrument measurement conditions.* According to the analysis principles of EDXRF, short-wavelength elements (light elements) choose low voltage and high current, and long-wavelength elements (heavy elements) choose high voltage and low current [26]. We defined Cr, Fe, and Mn as heavy elements; Si, P, and S as light elements; and V and Ti as medium elements. A sample with a high main content was placed on the turntable of the sample changer. Under the different condition groups, the percentage of dead time was controlled by changing the current value. As long as the value was around 30%, interference from the primary spectrum with the element could be removed, which improved the sensitivity of the analysis [27]. An Al-200 filter was chosen when analyzing for Cr, Fe, and Mn. Because the light elements were difficult to excite and their fluorescence energy was low, a lower tube pressure was selected, and the filter was not required to improve the excitation efficiency. The optimized instrument measurement conditions are shown in Table 1.

Spectrum line overlap interference and matrix effect correction. The calibration samples we prepared were used to measure fluorescence intensity under the optimized measurement conditions. The EDXRF spectrum of the ferrochromium is shown in Fig. 1. The X-ray peaks of Cr, Fe, Si, Mn, V, Ti, P, and S, along with coincident peaks, were observed in the

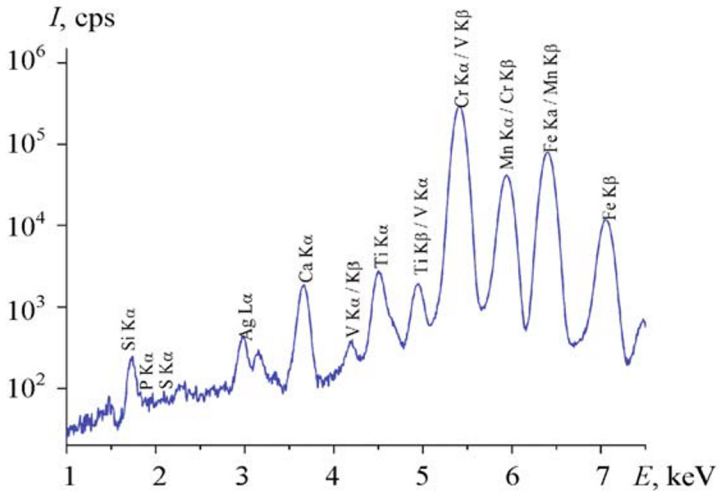

Fig. 1. Ferrochromium energy dispersive X-ray fluorescence spectrum.

TABLE 1. Optimized Instrument Measurement Conditions

Element	Analytical line	Voltage, kV	Current, μA	Measure time, s	Filter	Measurement environment	Detector mode
Cr	K_α	20	100	90	Al-200	Air	Normal
Fe	K_α	20	100	90	Al-200	Air	Normal
Mn	K_α	20	100	90	Al-200	Air	Normal
P	K_α	6	900	200	None	Helium	High resolution
S	K_α	6	900	200	None	Helium	High resolution
Si	K_α	6	900	200	None	Helium	High resolution
Ti	K_α	12	85	120	Al-50	Helium	High resolution
V	K_α	12	85	120	Al-50	Helium	High resolution

TABLE 2. Element Corrections

Element	Matrix correction elements	Overlapping elements
Fe	Cr, Mn, P, Si, Ti, V	–
Si	Cr, Fe, Mn, V, Ti, P	–
Mn	Fe, Si, Ti, V	Cr
V	Cr, Mn, Si, Ti, V	Ti
Ti	Cr	–
P	Cr, Fe, Mn, V, Ti	Si
S	Cr, Fe, Mn, V, Si, Ti	P

EDXRF spectrum of the standard. The overlap and interference of adjacent heavy elements were more serious, as shown in Fig. 1. Therefore, these interference elements had to be accounted for when performing the spectral line overlap interference correction.

TABLE 3. Calibration Curve Coefficients

Element	*D*	*E*	R^2	RMS	*K*
Cr	57.743	0.0000890	0.9922	0.00696	0.0919
Fe	13.635	0.00173	0.9961	0.00544	0.0978
Mn	0.423	0.000468	0.9995	0.000114	0.0165
V	−0.00510	0.00117	0.9986	0.0000474	0.00913
Ti	−0.0108	0.000575	0.9997	0.0000497	0.00831
Si	−0.0961	0.00119	0.9958	0.00175	0.129
P	−0.0279	0.000285	0.9912	0.0000232	0.00630
S	0.0160	0.0000950	0.9945	0.0000202	0.00543

TABLE 4. Selected Process Variable Levels

No.	Variable	Low level	Central point	High level
		−1	0	1
A	Sample quality (g)	3	5	7
B	Binder dosage (g)	0.3	0.5	0.7
C	Tablet pressure (MPa)	10	25	40

TABLE 5. Design of Experiments

No.	Variable			Element count rate (cps)							
	A	*B*	*C*	Cr	Fe	Si	Mn	V	Ti	P	S
1	7	0.7	40	109,833	33,814	6724	2172	280	615	331	991
2	5	0.5	25	109,520	33,430	6570	2173	281	599	315	966
3	7	0.3	10	111,886	33,852	7216	2197	285	616	217	951
4	7	0.3	40	112,946	34,409	7342	2210	299	617	219	905
5	3	0.7	10	100,841	30,830	4928	2016	245	548	439	960
6	3	0.3	40	110,132	33,400	6594	2170	280	601	323	967
7	5	0.5	25	109,032	33,370	6630	2150	277	609	321	992
8	3	0.3	10	107,894	32,550	6342	2143	277	589	303	966
9	7	0.7	10	106,805	32,702	6461	2111	272	600	311	988
10	3	0.7	40	102,391	31,782	52451	2053	249	553	479	955

This method used the empirical coefficient method to correct for the matrix effect, and it used multiple regression to correct the spectral line overlap interference. The appropriate K_α/K_β spectrum was selected according to the correlation coefficient, followed by adding the element spectrum that may have interfered with the element to generate the proper

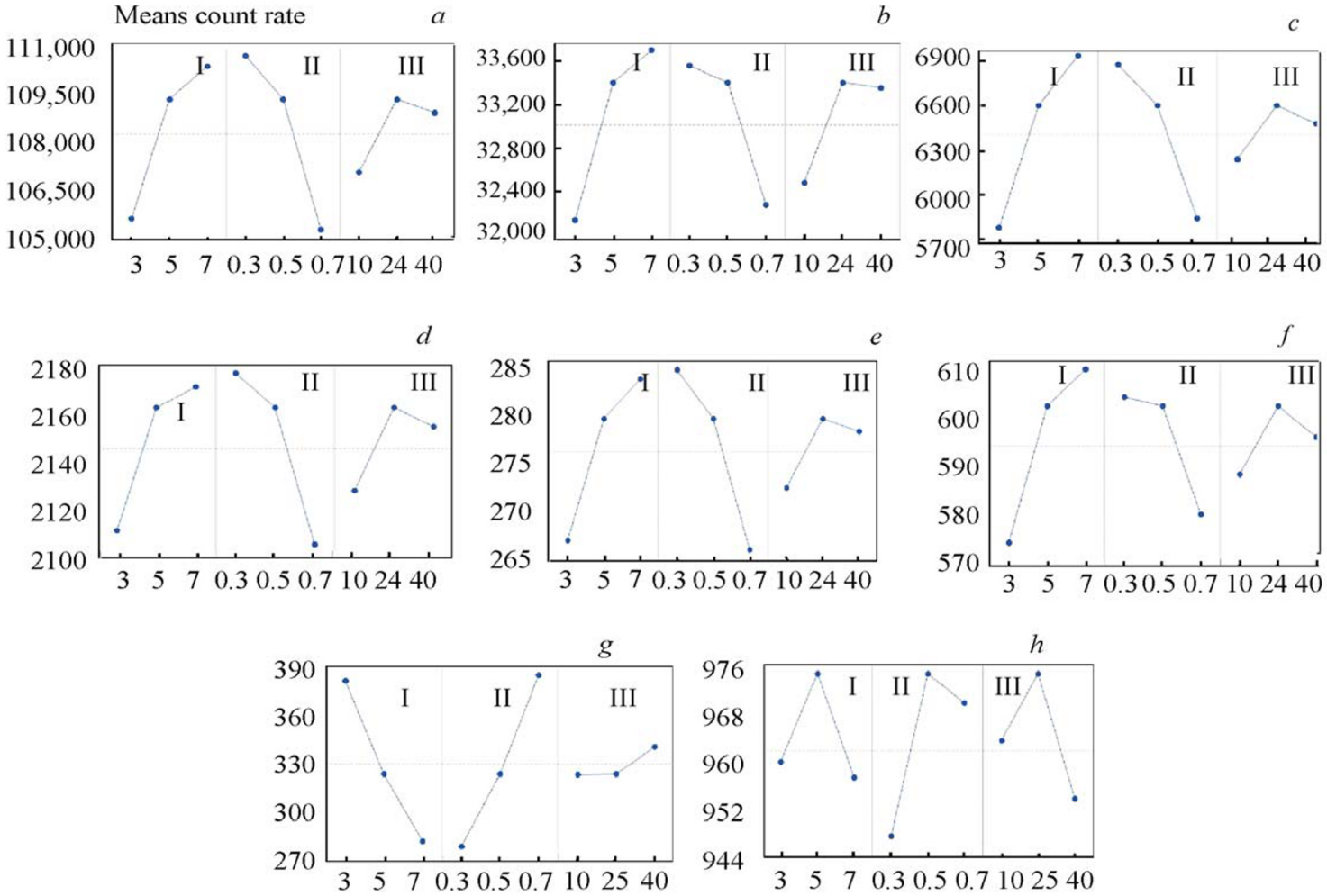

Fig. 2. Main effects of the influencing factors for Cr (a), Fe (b), Si (c), Mn (d), V (e), Ti (f), P (g), and S (h); I, sample quality; II, binder dosage; III, tablet pressure.

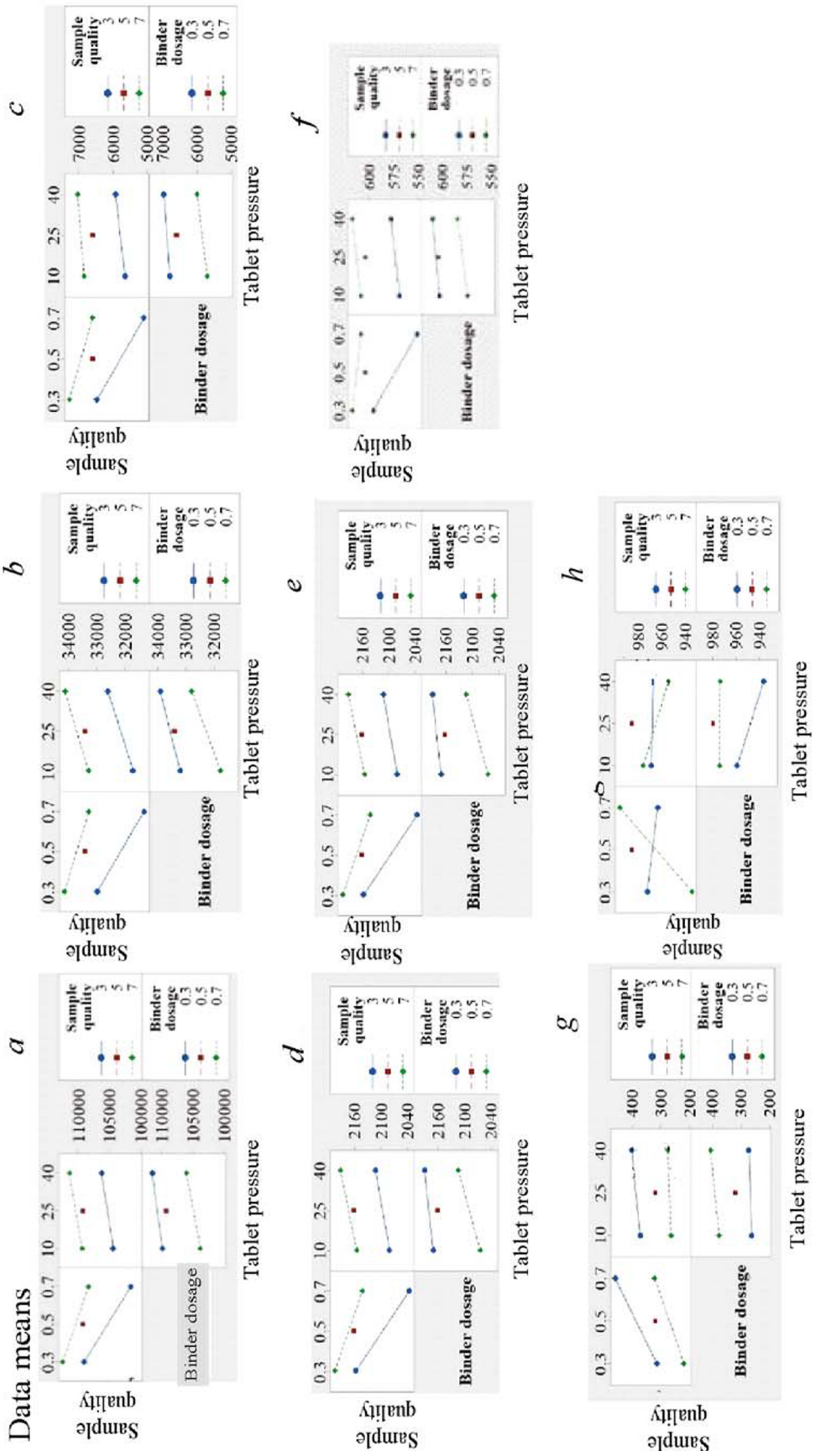

Fig. 3. Interactions of the influencing factors for Cr (a), Fe (b), Si (c), Mn (d), V (e), Ti (f), P (g), and S (h).

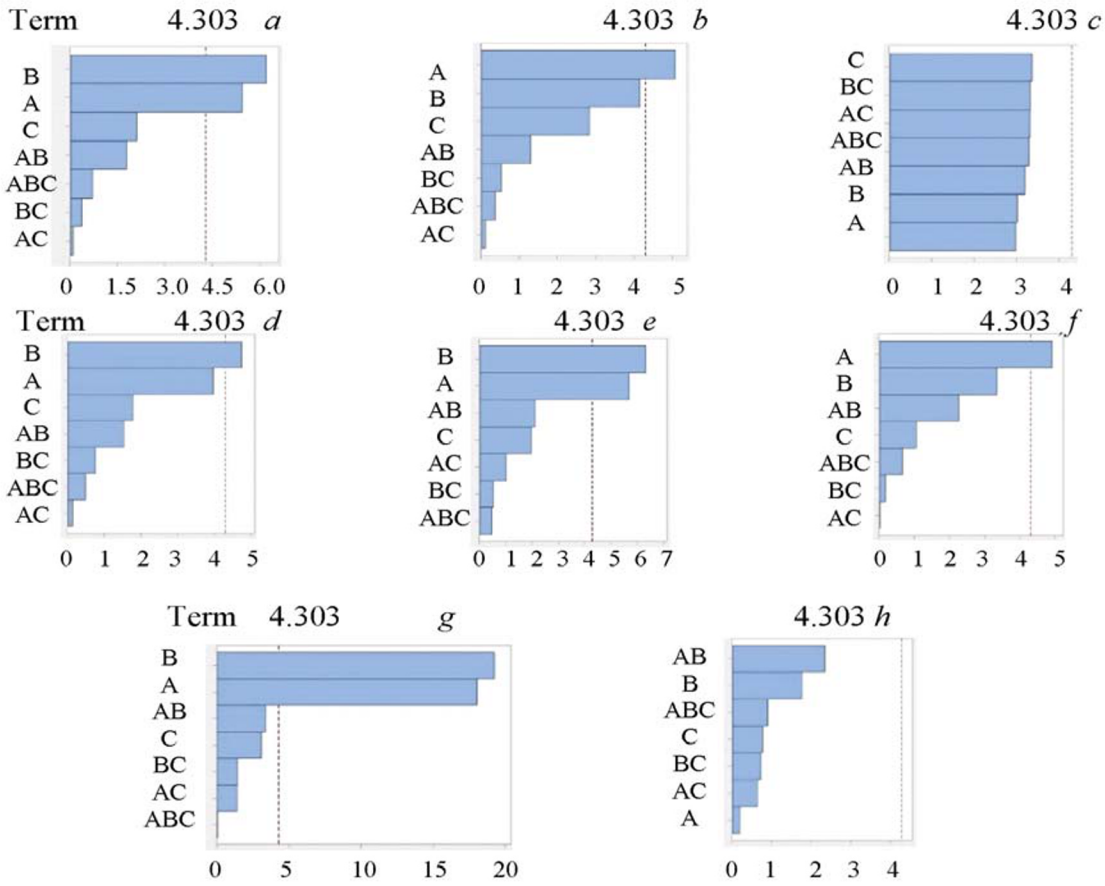

Fig. 4. Pareto chart of the influencing factors. A: sample quality; B: binder dosage; C: tablet pressure.

correction. We were able to avoid overcorrection, as evidenced by the negative intensity of the elements. Table 2 shows the corrections of the related elements.

Establishment of the standard curve. After carrying out the interference correction, the regression was repeated to gain the intercept, slope, matrix correction coefficient, and spectral line overlap interference correction coefficient of the calibration curve. The quality factor value (K), root-mean-square deviation (RMS), and correlation coefficient (R^2) were used to measure the quality of the standard curve. The smaller the K value, the RMS and the larger the correlation coefficient, the better the fit between the calculated value and the standard value. For components with a mass fraction >1%, the RMS was <1, and a K value of <0.5 was appropriate. For components with a mass fraction <1%, the RMS was <0.5, and a K value of <0.1 was appropriate. The calibration curve coefficients are presented in Table 3: K of each component was <0.129, the RMS was <0.00696, the correlation coefficients of the eight elements were all >0.99, and the linear correlation was good. These results suggested that the calibrated model was appropriate for establishing the standard curve.

Optimization of the sample preparation conditions. Optimization was performed using a full-factor experimental design that considered three variables: sample quality, binder dosage, and tablet pressure. All optimization experiments were performed in random order. The experimental data were processed using MINITAB 9.0 software to determine the optimal values of these variables. The variables and levels used in the DOE design are described in Table 4. The levels of the operating variables, analyte intensities, and response values are presented in Table 5.

Minitab 9.0 software was used for the DOE fitting, and the fitting direction was the maximum fluorescence intensity value. To visually express the relative strength of the main effects, interactions, and influencing factors for each factor, we prepared a main effects diagram and a Pareto diagram of the standardized effects of the interaction diagram, as shown in Figs. 2–4.

The influences of the variables on the responses were studied using a full-factor experiment. When measuring with the ferrochromium specimen, the binder dosage had the most influence on fluorescence intensity, followed by sample

TABLE 6. Results (content, wt.%) of the Method Precision Test (n = 5)

No.	Cr	Fe	Si	Mn	V	Ti	P	S
1	54.190	27.400	7.816	0.722	0.345	0.573	0.0190	0.0220
2	54.030	27.350	7.908	0.701	0.372	0.569	0.0210	0.0230
3	54.050	27.310	7.897	0.714	0.364	0.584	0.0190	0.0230
4	54.100	27.340	7.822	0.710	0.367	0.563	0.0210	0.0240
5	54.150	27.610	7.636	0.715	0.339	0.574	0.0190	0.0230
Average	54.104	27.402	7.820	0.712	0.357	0.573	0.0198	0.0230
RSD, %	0.12	0.44	1.39	1.08	4.06	1.35	5.53	3.07

TABLE 7. Results (content, wt.%) of the Instrument Precision Test (n = 11)

No.	Cr	Fe	Si	Mn	V	Ti	P	S
1	53.790	27.540	7.895	0.709	0.359	0.577	0.0210	0.0230
2	53.960	27.390	7.898	0.719	0.362	0.576	0.0200	0.0230
3	53.950	27.440	7.862	0.702	0.354	0.572	0.0210	0.0230
4	53.720	27.610	7.862	0.703	0.347	0.584	0.0200	0.0220
5	54.020	27.350	7.904	0.724	0.363	0.575	0.0220	0.0220
6	53.990	27.410	7.874	0.718	0.354	0.581	0.0210	0.0220
7	54.020	27.390	7.875	0.703	0.355	0.579	0.0210	0.0220
8	54.110	27.390	7.844	0.700	0.348	0.576	0.0210	0.0220
9	53.940	27.350	7.924	0.714	0.366	0.568	0.0220	0.0230
10	53.890	27.530	7.880	0.727	0.351	0.573	0.0210	0.0220
11	53.910	27.370	7.937	0.716	0.365	0.574	0.0220	0.0220
Average	53.936	27.434	7.887	0.712	0.357	0.576	0.0211	0.0224
RSD, %	0.20	0.32	0.35	1.32	1.88	1.32	3.32	2.26

quality and tablet pressure. The main effects were plotted (Fig. 2) to check the differences between the level averages of one or more factors. This showed that the fluorescence intensity decreased with increasing binder dosage, which was affected by each level of the parameters. The binder dosage was the major factor, with sample quality and tablet pressure being the second and third minor listed factors, respectively, that affected the fluorescence intensity. With a small binder dosage, the sample quality was abundant in order to increase measurement precision.

The two-way interaction plots shown in Fig. 3 indicate that one factor had an impact on the other factors. Because third-order interaction effects have many influencing factors, we did not analyze them here. As shown in Fig. 3, the interaction effect between the parameters of sample quality and binder dosage was significant for fluorescence intensity. This demonstrated that these three variables had an interaction effect on the determination of the Si and S contents. To screen the significant interference factors more intuitively from the investigation factors, a Pareto chart of the statistical analysis of the design was used to rank the magnitude and relative importance of the independent and interactive effects of each factor (Fig. 4). The vertical line in the Pareto chart indicated a statistically significant effect on the response for 5% significance level [21]. However, any effect that ranged past this datum was potentially important. Therefore, we concluded that a binder dosage, with the highest coefficient estimate and a $p < 0.05$, was the most important factor affecting the fluorescence intensity for the Cr, Fe, Si, and P elements, followed by sample quality. It is worth noting that no significant

TABLE 8. Analytic Results (content, wt.%) for the Certified Reference Materials YSBC28624-2010

Value	Cr	Fe	Mn	Si	V	Ti	P	S
Standard	60.00	28.65	0.34	2.43	0.153	0.261	0.025	0.033
EDXRF	60.29	28.07	0.32	2.40	0.145	0.261	0.024	0.032
ICP–AES	60.76	29.84	0.33	2.25	0.160	0.200	–	–

interaction effect was observed among the three independent variables investigated in this study, as evidenced by the high p value of all the two-factor interaction parameters ($p > 0.05$).

As the optimal conditions could not be obtained directly from the main effect diagram, a response optimizer was used to predict the maximum value of the corresponding value of the target. We set the weight and importance to 1, and the maximum fluorescence intensities of Cr, Fe, Si, Mn, V, and Ti as the targets. The response optimizer generated a response optimization diagram for the eight elements. The optimized conditions were as follows: sample weight 5 g, binder dosage 0.3 g, sample preparation pressure 40 MPa, and composite desirability of the fitting 0.89. After carrying out these experiments, the measured values of the major and minor components of the ferrochromium under this condition were more consistent with the certified values.

Method validation. Five ferrochromium samples were prepared in parallel to determine the precision of the measurement method. The relative standard deviation (RSD, %) of each component was between 0.12 and 5.53%. The instrument precision was calculated from 11 replications of the experiment under optimized conditions using ferrochromium samples of all eight elements ranging from 0.20 and 3.32%, as shown in Tables 6 and 7. The RSD of the determination result was <2% for major element content and <6% for the trace components. The results showed the high precision of this method, which indicated the possibility of continuous analysis.

Using this method, the ferrochrome standard material YSBC28624-2010, which had not been used for the regression, was used as an unknown material for powder compression sample preparation. The results showed that the measured values were consistent with the standard value range (Table 8), indicating that the method was accurate and could meet the requirements for the quantitative determination of the major and minor components of ferrochromium products. As calculated, the relative errors of the eight elements ranged from 0.49 to 5.29%. The ferrochrome samples used for the accuracy verification were melted according to the experimental method, and were measured by inductively coupled plasma emission spectrometry. The results are presented in Table 8. The EDXRF results were slightly better than traditional wet analysis in terms of accuracy and operation when analyzing ferrochromium. Therefore, the proposed procedure can be efficiently applied for the determination of elements in ferrochromium powder samples.

Conclusions. The proposed energy dispersive X-ray fluorescence analysis method for the determination of ferrochromium is extremely simple, rapid, sensitive, and reproducible. The response optimizer enabled us to obtain the optimal sample preparation conditions for the energy dispersive X-ray fluorescence determination of Cr, Fe, Si, Mn, V, Ti, P, and S in ferrochromium. The RSD values were <2.26%. The verification experiment showed that there was no significant difference between the measured value and the certified value. The time required for the entire preparation and analysis was only 15–20 min. Compared with wet analysis, this method is more suitable for the quantitative analysis of high-carbon ferrochromium powder samples.

Acknowledgments. This work was financially supported by the National Nature Science Foundation of China (No. U1607103), and the Natural Science Foundation in Qinghai Province (No. 2019-ZJ-940Q).

REFERENCES

1. V. A. Maslyuk, R. V. Yakovenko, O. A. Potazhevskaya, and A. A. Bondar, *Powder Metall. Met. Ceram*., **52**, 47–57 (2013).
2. N. Sasaguri, K. Yamamoto, Y. Yokomizo, and Y. Matsubara, *Mater. Trans*., **60**, 2537–2541 (2019).
3. J. Wang, G. Hu, Z. Peng, and K. Du, *Trans. Nonferrous Met. Soc. China*, **25**, 3820–3826 (2015).
4. B. Lu, C. Zhang, Z. Guo, F. Yang, H. Y. Wang, A. Volinsky, and Y. Li, *J. Mater. Eng. Perform*., **28**, 5361–5368 (2019).
5. P. Kumar, N. Sahu, A. Roshan, B. N. Rout, and S. K. Tripathy, *Min. Proc. Ext. Met. Rev*., 1–11 (**2021**).

6. B. Li, P. Han, B. Zhang, H. T. Feng, W. Li, and Y. P. Dong, *J. Hazard Mater*., **387**, Article ID 121699 (2020).
7. Z. L. Gu, *Shandong Metall*., **43**, 48–49 (2021).
8. D. X. Hu, K. Xiao, X. D. Wang, Z. K. Wang, M. Liu, and Q. B. Li, *Rock Miner. Analysis*, **33**, 208–211 (2014).
9. I. I. Chernikova, K. V. Tumneva, T. V. Bakaldina, and T. N. Ermolaeva, *Inorg. Mater*., **56**, 1384–1390 (2020).
10. I. Hlaváček and I. Hlaváčková, *Anal. At. Spectrom*., **6**, 535–540 (1991).
11. I. I. Chernikova, K. Y. Tumneva, T. Y. Bakaldina, and T. N. Ermolaeva, *Ind. Lab. (Diagn. Mater.)*, **85**, 11–17 (2019).
12. R. Mittal, P. Rao, and P. A. Kaur, *J. Appl. Spectrosc*., **84**, 1131–1138 (2018).
13. Y. L. Liu, Q. X. Zhang, J. Zhang, H. T. Bai, and L. Q. Ge, *Nucl. Sci. Technol*., **30**, 1–11 (2019).
14. A. A. Shaltout, M. M. Dabi, M. M. Ibrahim, S. Ahmed, and E. B. Essam, *Trace Elem. Res*., **195**, 417–426 (2020).
15. P. Rao and R. Mittal, *J. Appl. Spectrosc*., **87**, 1185–1195 (2021).
16. M. F. Gülcan, B. D. Karahan, and S. J. Gürmen, *Mater. Res. Technol*., **9**, 14103–14115 (2020).
17. A. G. Coedo, T. Dorado, C. J. Rivero, and G. C. Isabel, *J. Anal. At. Spectrom*., **8**, 1023–1027 (1993).
18. G. Wang, J. Diao, L. Liu, M. Li, H. Y. Li, G. Li, and B. Xie, *J. Cleaner Prod*., **237**, Article ID 117832 (2019).
19. M. Büyükyıldız, E. Boydaş, M. Kurudirek, and E. Öz Orhan, *Instrum. Exp. Technol*., **60**, 584–588 (2017).
20. N. X. Gao, *J. Appl. Spectrosc*., **87**, 326–332 (2020).
21. E. Hazir, E. S. Erdinler, and K. H. Koc, *J. For. Res*., **29**, 1423–1434 (2018).
22. G. Kishore, A. Parthiban, A. R. Sivaram, and V. Vijayan, *Mater. Today: Proc.*, **37**, 3256–3261 (2021).
23. M. G. Arafa and B. M. Ayoub, *Sci. Rep*., **7**, 1–15 (2017).
24. V. de Jesus Ferreira, J. S. Almeida, V. A. Lemos, O. M. C. de Oliveira, K. S. Larsia, and L. S. G. Teixeira, *Talanta*, **222**, Article ID 121514 (2021).
25. X. Q. Li, H. T. Feng, B. Li, D. D. Gao, B. Zhang, Y. P. Dong, and W. Li, *J. Salt Lake Res*., **29**, 102–108 (2021).
26. T. R. Tavares, J. P. Molin, L. C. Nunes, E. E. Alves, F. L. Melquiades, H. W. Carvalho, and A. Mouazen, *Remote Sens*., **12**, 963 (2020).
27. P. Bachiega, E. de Almeidia, J. M. Salgado, M. A. Z. Arruda, E. L. Lehmann, M. C. Morzelle, and H. W. P. de Carvalho, *Food Anal. Method*, **12**, No. 7, 1520–1527 (2019).